Appl. Phys. A 88, 731–736 (2007)
DOI: 10.1007/s00339-007-4051-4

Applied Physics A
Materials Science & Processing

JEONG HO RYU[1,✉]
GYEONG SEON PARK[2]
KANG MIN KIM[2]
CHANG SUNG LIM[3]
JONG-WON YOON[2]
KWANG BO SHIM[2]

Synthesis of $CaWO_4$ nanocolloidal suspension via pulsed laser ablation and its optical properties

[1] Electro Materials & Device Center, Corporate R&D Institute, Samsung Electro-Mechanics Co., LTD., 314, Maetan 3-Dong, Yeongtong-Gu, Suwon-City, Guunggi-Do 443-743, South Korea
[2] Division of Advanced Materials Science Engineering, Hanyang University, 17 Haengdang-Dong, Seongdong-Gu, Seoul 133-791, South Korea
[3] Department of Advanced Materials Science and Engineering, Hanseo University, Seosan 356-706, South Korea

Received: 19 March 2007/Accepted: 14 April 2007
Published online: 14 June 2007 •

ABSTRACT Pulsed laser ablation (PLA) in the liquid phase was successfully employed to synthesize calcium tungstate ($CaWO_4$) nanocolloidal suspension. The crystalline phase, particle morphology and laser ablation mechanism for the colloidal nanoparticles were investigated using XRD, TEM and SEM. The obtained colloidal suspension consisted of well-dispersed $CaWO_4$ nanoparticles which showed a spherical shape with sizes ranging from 5 to 30 nm. The laser ablation and the nanoparticle forming process were discussed under consideration of the photo-ablation mechanism, where the nanoparticles were generated by rapid condensation of the plume in high pressured ethanol vapor. The optical properties of the prepared $CaWO_4$ colloidal nanoparticles were analyzed in detail using XPS, Raman spectroscopy, UV-Vis spectroscopy and PL spectrophotometry. The optical band gap was estimated by Tauc and Menths law.

PACS 42.62.-b; 82.70.Dd; 78.55.Hx; 81.07.Wx

1 Introduction

The synthesis and electro-optical properties of scheelite-type metal tungstates have been intensively investigated during the past half century [1–3]. In particular, calcium tungstate ($CaWO_4$) has attracted particular attention because it has been found to have practical importance as a MASER material [4–6], and as a scintillator [7, 8], in quantum electronics and medical applications. The $CaWO_4$ single crystals and polycrystalline powder have been prepared by several techniques such as the Czochralski method [9, 10], precipitation route [11, 12], hydrothermal synthesis [13] and solid-state reactions [14, 15]. However, $CaWO_4$ particles prepared by these processes are relatively large with irregular morphology, and inhomogeneous compounds might be easily formed because WO_3 have a tendency to vaporize at high temperatures [16]. To overcome this problem, extensive efforts have been made recently to develop alternative synthesis methods such as wet chemical routes [17], spray pyrolysis [18] or pulsed laser deposition (PLD) process [19].

Recently, pulsed laser ablation (PLA) of targets in liquids has attracted much attention as a new technique to prepare nanocolloidal particles since Henglein, Cotton and their coworkers first developed this synthesis technique [20, 21]. It has been demonstrated that laser ablation of various noble metals settled in solvents can produce colloidal nanoparticles of these metals [22–24]. A remarkable advantage of this laser ablation method over chemical synthesis is the simplicity of the preparation procedures. Furthermore, it has shown that the laser ablation in liquids is applicable to preparation of nanoparticles of not only noble metals but also compound materials, for example, TiO_2, ZnSe, GaAs and CoO in various solvents [25–28]. These studies of the laser ablation of noble metals and compound materials in liquid showed the formation of stoichiometric nanoparticles, i.e., atomic compositions of the produced nanoparticles were identical to those of the source materials.

In this work, we present a new synthetic approach to directly produce highly-dispersed $CaWO_4$ nanocolloidal suspensions using pulsed laser ablation (PLA) of ceramic targets in the liquid phase without any surfactant. The crystalline phase, surface morphology and optical properties were investigated. Moreover, laser ablation mechanisms and nanoparticle forming processes are discussed under consideration of photo-ablation mechanism.

2 Experimental

A fourth harmonic (266 nm) Nd:YAG pulse laser (Quentel, France) with a repetition rate of 30 Hz, pulse width of 8 ns and a maximum output of 100 mJ/pulse was used for synthesis of the $CaWO_4$ nanocolloidal suspension. The laser beam strikes the surface vertically after passing throughout an optical window and the liquid. Figure 1 shows

(a) a schematic diagram of the laser ablation process in liquid phase and
(b) an experimental view of the $CaWO_4$ target during laser ablation in ethanol.

✉ Fax: +82-31-300-7900, E-mail: jimihen.ryu@samsung.com

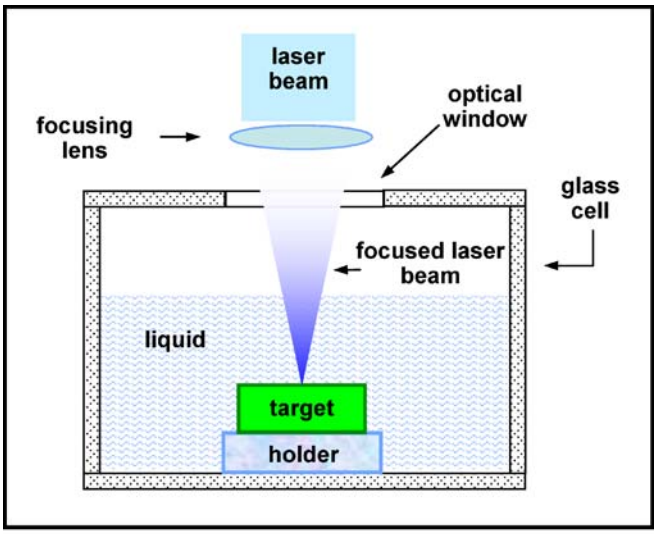

a

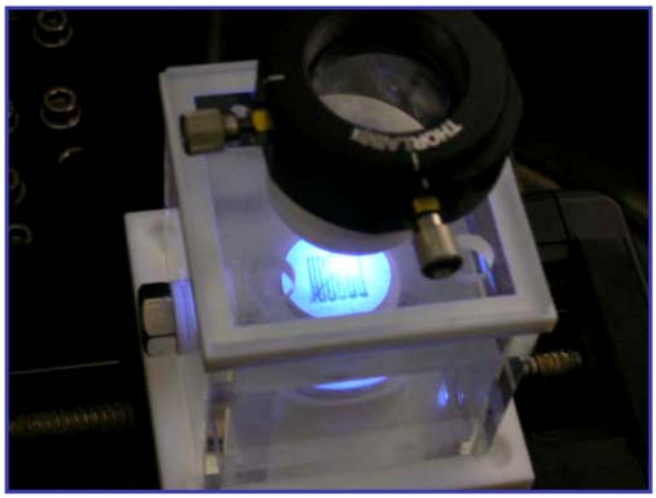

b

FIGURE 1 (**a**) Schematic diagram for laser ablation process in liquid phase and (**b**) experimental view of the $CaWO_4$ target during laser ablation in ethanol

To avoid the formation of deep holes in the target, the glass cell was displaced under the laser beam using a computer-driven X-Y stage with a laser scanning velocity of 0.5 mm/sec and 70%–80% overlaps of the laser spot among the consecutive scans.

The $CaWO_4$ powders were prepared via a citrate complex route [29] and the target was prepared by compressing the raw powders under a uni-axial pressure of 300 MPa, and then by sintering at 900 °C in air for 3 h. The prepared $CaWO_4$ target was white–yellow in color. The crystalline phase of the target was identified by XRD, showing a single phase which was consistent with reported values (inset of Fig. 2a, JCPDS Cards 41-1431). After removing organic contaminations with ultrasonic cleaning in acetone, the cleaned target was immersed into 60 ml ethanol, thereafter the target was irradiated by the Nd:YAG pulsed laser. The laser beam was focused on the target with a beam size of about 1 mm in diameter using a lens with a focal length of 50 mm. The depth of the target immersed into the ethanol was kept to about 20 mm. The colloidal suspension was prepared by laser ablation for 6 h at room temperature.

Surface morphology of the $CaWO_4$ target was observed after laser ablation using a scanning electron microscope (SEM, JEOL, JSM 5900 LV, Japan) for investigating the laser ablation mechanism. The microstructure and shape of the colloidal nanoparticles were investigated using transmission electron microscopy (TEM, JEOL, JEM-2010, 200 kV, Japan) after dropping the colloidal suspension on a carbon-coated copper grid. Precipitates of the products were formed by repeated centrifuging at 25 000 rpm for 30 min. using an ultracentrifuge (Supra 25K, Hanil Sci., Korea). For the measurements of X-ray diffraction (XRD, CuKα, 40 kV, 30 mA, Rigaku, Japan) the precipitates of the suspensions were dried on the glass substrate. The surface chemical states of the prepared nanoparticles were analyzed using X-ray photoelectron spectroscopy (XPS, PHI 5600ci, USA) with a monochromated Al−Kα source (1486.5 eV, 100 W). The typical pass energy and the energy resolution were 5.85 eV and 0.05 V/step, respectively. The binding energy values were calibrated with the C 1 s line of adventitious carbon at 284.5 eV. The Raman spectrum was recorded on a dispersive laser spectrophotometer (NRS-3100, JASCO) with an excitation wavelength of 633 nm. Subsequently, the optical absorption and photoluminescence (PL) spectrum of the $CaWO_4$ nanoparticles-dispersed colloid were measured using an UV-Vis spectrophotometer (Optizen 2120 UV, Mecasys, Korea) and a luminescence spectrometer (PerkinElmer LS45, USA) at room temperature.

3 Results and discussion

3.1 *Laser induced formation of nanoparticles and the ablation mechanism*

Figure 2a shows XRD pattern of the $CaWO_4$ nanoparticles collected from a colloidal suspension prepared by pulsed laser ablation in ethanol. The Bragg reflection peaks of the nanoparticles correspond to the scheelite structured $CaWO_4$ without any peaks assigned to Ca, CaO, $CaCO_3$, W, or WO_3 phases. The broad reflection peaks in Fig. 2a indicate the formation of very small nanoparticles. The average crystallite size of the synthesized nanoparticles was estimated from the XRD peak width of (111) based on Scherrers formula [30], $D = k\lambda/\beta\cos\theta$, where D is the average particle size, k is a constant equal to 0.89, λ is the wavelength of X-rays equal to 0.1542 nm (i.e. Cu−Kα) and β the corrected half-width that is obtained by using the (111) line of pure silicon as the standard. The calculated average crystallite size of the $CaWO_4$ nanoparticles was 14 nm. The particle morphology, particle size and crystallinity were observed more closely by TEM as shown in Fig. 2b. The morphology of the nanoparticles was spherical and uniform with diameters between 5 and 30 nm. Selected area electron diffraction (SAED) patterns shown in Fig. 2c revealed bright polycrystalline diffraction rings, and lattice spacings derived from the diffraction rings in agreement with the scheelite structured $CaWO_4$.

Figure 3 shows typical SEM micrographs of the $CaWO_4$ target surface before laser ablation (a) and after laser ablation (b) showing remarkable changes of the surface morphology induced by the laser ablation. The laser ablation of solids in

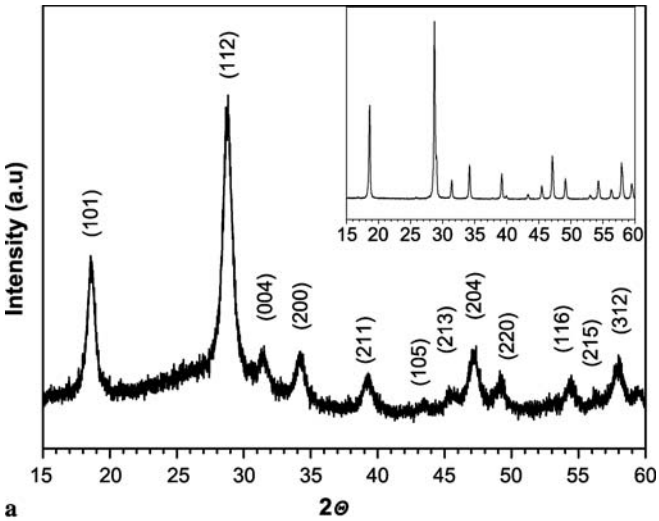

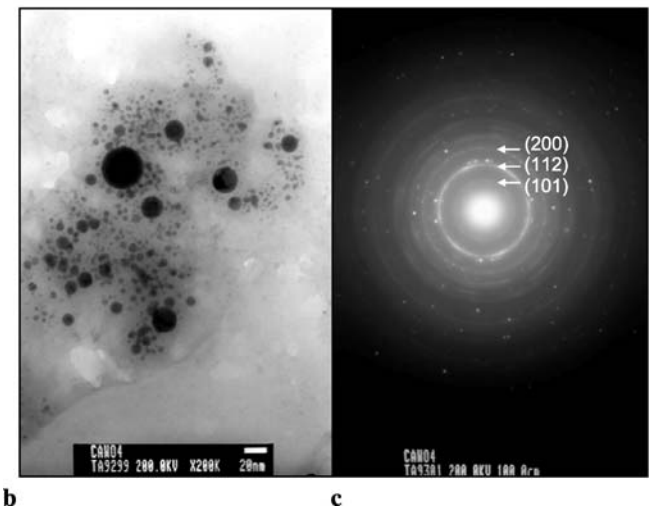

FIGURE 2 (**a**) X-ray diffraction patterns of the $CaWO_4$ nanoparticles collected from the colloidal suspension. The XRD patterns of the targets are shown in the *inset*. (**b**) TEM images of the $CaWO_4$ nanoparticles prepared by pulsed laser ablation in ethanol. The selected electronic diffraction patterns corresponding to (**b**) are shown in (**c**)

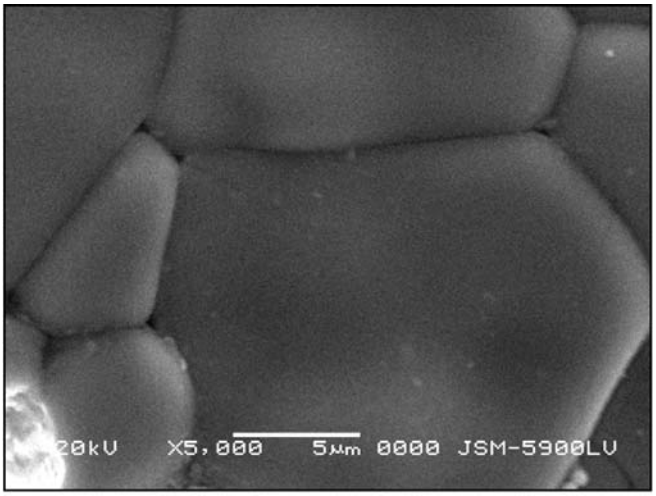

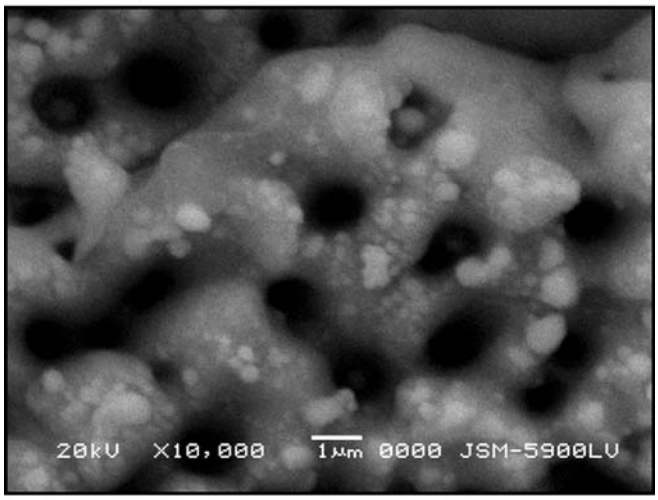

FIGURE 3 Typical SEM micrographs of the $CaWO_4$ target (**a**) before and (**b**) after laser ablation showing the remarkable change of the surface morphology induced by the laser irradiation

a liquid medium occurs when a high-power laser beam is focused at the submerged target surface for an appropriate time, and leads to ejection of nanoparticles into the liquid where they are condensed and cooled. Molecular dynamics simulations [31–34] have proposed two different mechanisms of particle removal during laser ablation. Below a given threshold of laser fluence, there is desorption of small clusters. However, above this threshold of laser fluence, the ejected plume contains a substantial fraction of large molecular clusters due to the induced photo-ablation of the target material.

In this case, the formation of the $CaWO_4$ nanoparticles via the PLA process can be considered as strong interactions between the ejected plume and surrounding ethanol molecules above the threshold of laser fluence. Microscopic observation of the changes of the target surface as shown in Fig. 3, indicates that the threshold of laser fluence was surpassed. During the laser irradiation, a thin layer of the target is heated well above its melting temperature, while the adjacent ethanol molecules are heated to the same temperature by the heat transfer from the interface [31]. Considering the heat diffusion coefficient in ethanol of $a = 10^{-3}$ cm^2/s and the diffusion time is approximately equal to the duration of one laser pulse ($t_p = 8$ ns), the thickness of the heated liquid layer h is approximately $\sim (at_p)^{1/2} = 0.028$ μm. After just 10 pulses at the same focal point, i.e. after only 0.33 s, the estimated ethanol bubble has a radius of about 0.9 μm. This radius is much greater than the particle size verified in the TEM result.

Therefore, the ablation process can be described with a photo-ablation process [31–34] where the $CaWO_4$ nanoparticles are formed by condensation of an ablated plume in an ethanol vapor medium. This means that the ablation process in ethanol is not very different from those occurring in thin film growth processes at normal atmosphere, with just one important difference, that the pressure in the bubbles is very high [31]. The interaction between the plume and the high pressured ethanol vapor leads to fast condensation and agglomeration of clusters. In the case of ablation due to desorption of small clusters, i.e. when below the threshold of laser fluence, the surface of laser ablated target should be more flat and less rough [31–34]. It seems that this is not the case here. Therefore, the particles observed in Fig. 2b with diam-

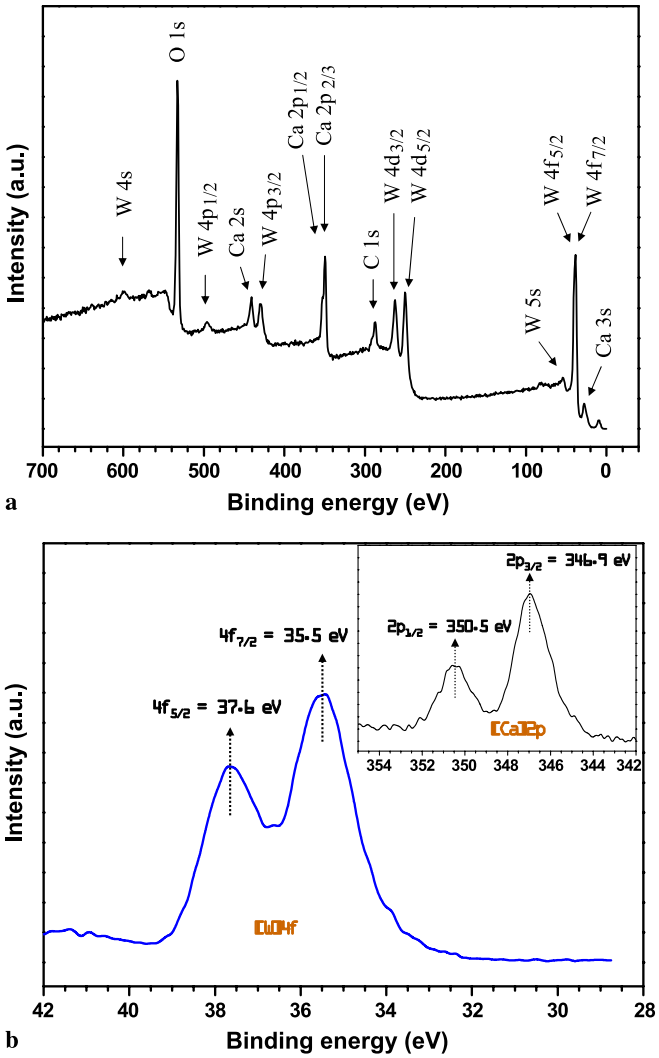

FIGURE 4 (**a**) XPS wide scan spectrum and (**b**) high resolution [W] 4f doublet peaks of the $CaWO_4$ colloidal nanoparticles. The [Ca] 2p energy region is depicted in *inset* of (**b**)

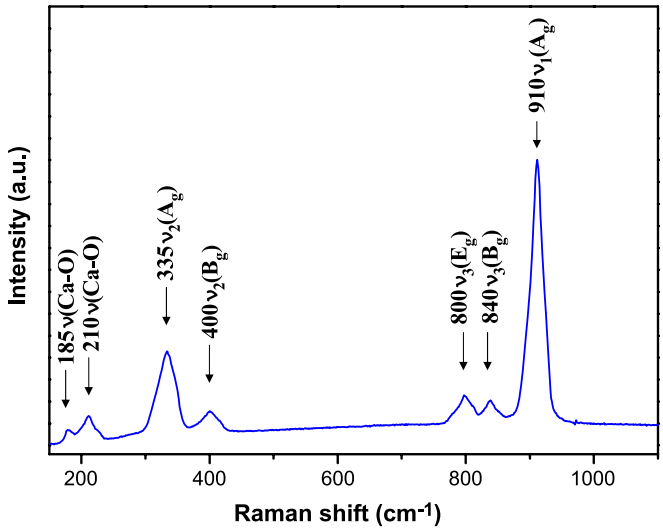

FIGURE 5 Raman spectrum of the $CaWO_4$ nanoparticles collected from the colloidal suspension

eters between 5 and 50 are thought to result from condensed clusters or larger recast droplets fragmented from the target.

3.2 *Optical properties of the prepared* $CaWO_4$ *colloidal nanocrystals*

The surface composition of the $CaWO_4$ nanoparticles collected from the colloidal suspension prepared by pulsed laser ablation in ethanol was analyzed using XPS. Figure 4a shows an XPS wide scan spectra of the $CaWO_4$ nanoparticles. As shown in the wide scan of Fig. 4a, any metallic or organic impurities were not detected except for adsorbed carbon on the surface. Figure 4b shows the high resolution XPS spectra of the [Ca] 2p and [W] 4f regions of the $CaWO_4$ nanoparticles. The binding energies and branching ratio of the [Ca] $2p_{1/2}$ and $2p_{3/2}$ spin-orbit doublet at 350.5 and 346.9 eV are identical to the reported oxidized states of the [Ca] [35, 36] as shown in inset. The [W] 4f core level spectrum shows the two components associated with $4f_{5/2}$ and $4f_{7/2}$ spin-orbit doublet at 37.6 and 35.5 eV, respectively. These values agree with those found in the literature for $[W^{6+}]$ in stoichiometric films [37, 38]. Other peaks are shifted towards a lower binding energy, which is caused by contributions of $[W^{5+}]$ or $[W^{4+}]$ states resulting from oxygen vacancies [38], that were not detected.

Figure 5 shows the Raman spectrum of the $CaWO_4$ nanoparticles collected from a colloidal suspension prepared by pulsed laser ablation in ethanol. The $\nu_1(A_g)$ vibrations as a strong band is observed at 910 cm^{-1}, while the $\nu_2(A_g)$ vibrations are observed at 335 cm^{-1} accompanying a weak $\nu_2(B_g)$ at 400 cm^{-1}. The $\nu_3(B_g)$ vibration of $CaWO_4$ is located around 840 cm^{-1}, and the $\nu_3(E_g)$ is found at 800 cm^{-1}. These results are consistent with those reported previously [39–42]. In addition, the bands at 185 and 210 cm^{-1} can be assigned to the translational mode of the ν(Ca−O) and $[WO_4]^{2-}$ group in $CaWO_4$ [43], respectively.

Optical absorption spectrum of the $CaWO_4$ nanocolloidal suspension is presented in the inset of Fig. 6a. The sharp spectrum with high absorbance in the UV region proves the formation of a stable colloidal suspension consisting of well-dispersed $CaWO_4$ nanoparticles. The absorption spectrum showed a typical absorption edge near 250 nm. The optical band gap, E_{gap}, for the $CaWO_4$ colloidal nanoparticles was determined from the sharply increasing absorption region. According to Tauc and Menths law [44], the absorption coefficient has the following energy dependence, $(\alpha h\nu) = A(h\nu - E_{gap})^m$, where A is a proportionality constant, m is another constant, which is different for the transition types ($m = 1/2, 2, 3/2$ or 3 for allowed direct, allowed indirect, forbidden direct and forbidden indirect electronic transitions, respectively), $h\nu$ is the photon energy, and E_{gap} is the Tauc optical energy band gap. Therefore, the straight line plot between $(\alpha h\nu)^{1/m}$ and $h\nu$ would yield the value of the Tauc optical band gap (E_{gap}). The plot of $(\alpha h\nu)^2$ vs. photon energy $h\nu$ for the $CaWO_4$ nanocolloidal suspension is shown in Fig. 6a. In the low energy region of the edge, the absorption spectrum deviated from the straight line plot. However, in the high energy region of the absorption edge, $(\alpha h\nu)^2$ varied linearly with photon energy $h\nu$. This straight line behavior in the high energy region was taken as a prime evidence for the direct band gap.

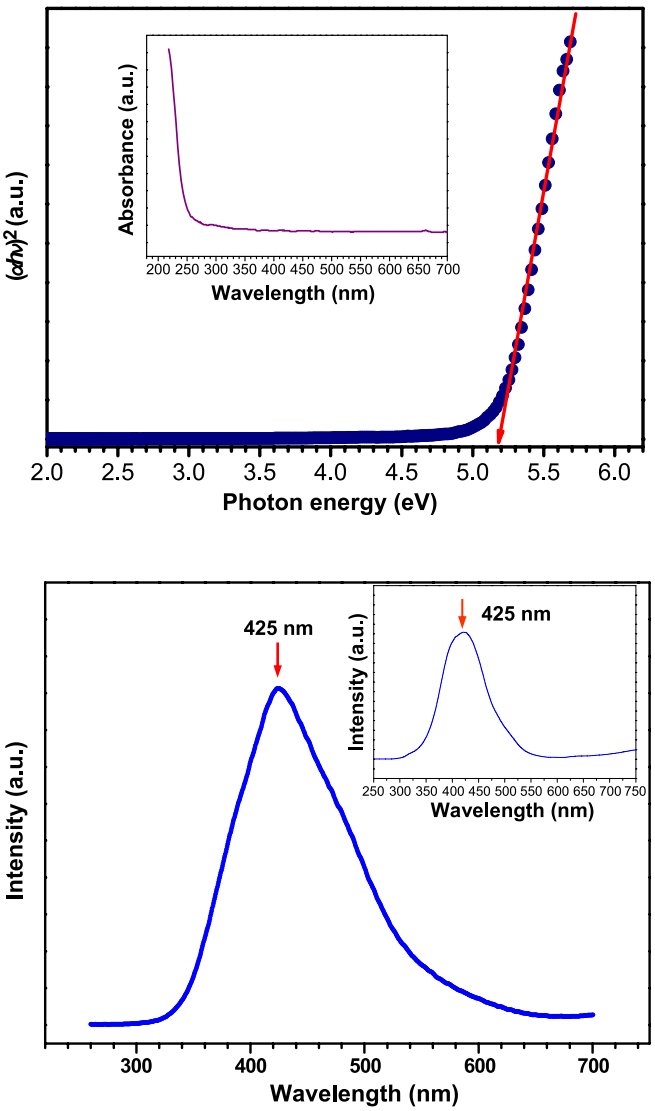

FIGURE 6 (**a**) Plot of $(\alpha h\nu)^2$ vs. $h\nu$ and UV-visible spectrum of the $CaWO_4$ nanocolloidal suspension prepared by laser ablation in ethanol (*inset*). The optical energy band gap is deduced from the extrapolation of the *straight line* up to $(\alpha h\nu)^2 = 0$. (**b**) Room-temperature PL emission spectrum of the prepared $CaWO_4$ nanocolloidal suspension. For comparison, the room-temperature PL spectrum of the bulk ceramic target is shown in *inset*

The optical band-gap was therefore determined by extrapolating the linear portion of the plot relating, $(\alpha h\nu)^2$ vs. $h\nu$ to $(\alpha h\nu)^2 = 0$ (see Fig. 6a). The estimated optical band gap was 5.19 eV, which is close to reported values, 5.4 eV by Saito et al. [45] and 5.27 eV by Maurera et al. [46].

The room-temperature PL emission spectrum of the $CaWO_4$ colloidal nanoparticles is shown in Fig. 6b. The PL emission spectrum was obtained at excitation of 240 nm. It is well known that $CaWO_4$ shows emission in the blue or green regions depending on excitation wavelength or energy [1–3]. In particular, optical band-edge excitation yields a strong blue emission and near-band-edge excitation yields a green emission [4–7]. Most of the studies on room-temperature PL for $CaWO_4$ crystals reported a blue emission around 420 nm for excitation between 240 and 280 nm and a green emission around 510 and 540 nm for excitation between 300 and 315 nm [8–10]. In Fig. 6b, the $CaWO_4$ colloidal nanoparticles show a broad intrinsic emission at 425 nm at room temperature. The inset of Fig. 6b shows the room-temperature PL spectrum of the bulk ceramic target to compare with the colloidal nanoparticles. Based on the single photoluminescent feature in Fig. 6b, it is proposed that the prepared $CaWO_4$ colloidal nanoparticles are stoichiometric and defect-free [47, 48]. Therefore these optical properties of the $CaWO_4$ nanocolloidal suspension may be utilized for a fluorescent device or biosensing applications.

4 Summary

A $CaWO_4$ nanocolloidal suspension was successfully synthesized using pulsed laser ablation in ethanol without any surfactant. The XRD, TEM, XPS, Raman, UV-Vis and PL results showed the synthesized $CaWO_4$ nanoparticles had a crystallized scheelite phase and highly uniform morphology with a spherical shape. The mechanism of laser ablation and nanoparticle formation was described by a photo-ablation process, where the nanoparticles were generated by rapid condensation of the ablation plume in a high pressured ethanol vapor. Therefore, the synthesis process of the $CaWO_4$ colloidal nanoparticles could be interpreted as being similar to thin film growth processes occurring under high-pressure conditions. The optical band gap of the $CaWO_4$ colloidal nanoparticles estimated by Tauc and Menths law was 5.19 eV. The $CaWO_4$ colloidal nanoparticles showed a broad single emission peak at 425 nm, which proves that the prepared $CaWO_4$ colloidal nanoparticles are stoichiometric and defect-free. It should be noted that this is a new approach for room-temperature synthesis of highly-dispersed $CaWO_4$ nanocolloidal suspension.

REFERENCES

1 R. Grasser, A. Scharmann, K.-R. Strack, J. Luminesc. **27**, 263 (1982)
2 M.J. Treadaway, R.C. Powell, J. Chem. Phys. **61**, 4003 (1974)
3 G. Born, A. Hofstaetter, A. Scharmann, G. Schwarz, J. Luminesc. **1**, 641 (1970)
4 A. Yariv, S.P.S. Porto, K. Nassau, J. Appl. Phys. **33**, 2519 (1962)
5 L.F. Johnson, G.D. Boyd, K. Nassau, R.R. Soden, Phys. Rev. **126**, 1406 (1962)
6 L.F. Johnson, R.A. Thomas, Phys. Rev. **131**, 2038 (1963)
7 J.W. Coltman, E.G. Ebbighausen, W. Altar, J. Appl. Phys. **18**, 530 (1947)
8 D.R. Shearer, L.E. Rowe, Med. Phys. **14**, 197 (1987)
9 A.R. Chaudhuri, L.E. Phaneuf, J. Appl. Phys. **34**, 2162 (1963)
10 C.D. Brandle, J. Cryst. Growth **264**, 593 (2004)
11 A. Sen, P. Pramanik, J. Eur. Ceram. Soc. **21**, 745 (2001)
12 V. Thangadurai, C. Knittlmayer, W. Weppner, Mater. Sci. Eng. B **106**, 228 (2004)
13 J.T. Kloprogge, M.L. Weier, L.V. Duong, R.L. Frost, Mater. Chem. Phys. **88**, 438 (2004)
14 G. Bayer, H.-G. Wiedemann, Thermochim. Acta **133**, 125 (1988)
15 R.B. Pode, S.J. Dhoble, Phys. Stat. Solidi B **203**, 571 (1997)
16 W.S. Cho, M. Yashima, M. Kakihana, A. Kudo, T. Sakata, M. Yoshimura, J. Am. Ceram. Soc. **80**, 765 (1997)
17 P.Y. Jia, X.M. Liu, G.Z. Li, M. Yu, J. Fang, J. Lin, Nanotechnology **17**, 734 (2006)
18 Z. Lou, M. Cocivera, Mater. Res. Bull. **37**, 1573 (2002)
19 K. Tanaka, D. Fukui, K. Ohga, C.-K. Choo, J. Vac. Sci. Technol. A **20**, 486 (2002)
20 A. Fojtik, A. Henglein, Ber. Bunsenges. Phys. Chem. **97**, 252 (1993)
21 J. Heddersen, G. Chumanov, T.M. Cotton, Appl. Spectrosc. **47**, 1959 (1993)
22 A.V. Simakin, V.V. Voronov, G.A. Shafeev, R. Brayner, F.B. Verduraz, Chem. Phys. Lett. **348**, 182 (2001)
23 R.A. Ganeev, M. Baba, A.I. Ryasnyansky, M. Suzuki, H. Kuroda, Opt. Commun. **240**, 437 (2004)

24 G.A. Shafeev, E. Freysz, F.B. Verduraz, Appl. Phys. A **78**, 307 (2004)
25 A. Iwabuchi, C.-K. Choo, K. Tanaka, J. Phys. Chem. B **108**, 10 863 (2004)
26 K.V. Anikin, N.N. Melnik, A.V. Simakin, G.A. Shafeev, V.V. Voronov, A.G. Vitukhnovsky, Chem. Phys. Lett. **366**, 357 (2002)
27 R.A. Ganeev, M. Bara, A.I. Ryasnyansky, M. Suzuki, H. Kuroda, Appl. Phys. B **80**, 595 (2005)
28 T. Tsuji, T. Hamagami, T. Kawamura, J. Yamaki, M. Tsuji, Appl. Surf. Sci. **243**, 214 (2005)
29 J.H. Ryu, J.-W. Yoon, C.S. Lim, W.-C. Oh, K.B. Shim, Ceram. Int. **31**, 883 (2005)
30 B.D. Cullity, S.R. Stock, *Elements of X-ray Diffraction*, 3rd edn. (Prentice-Hall, Upper Saddle River, New Jersey, 2001)
31 M.S.F. Lima, F.P. Ladário, R. Riva, Appl. Surf. Sci. **252**, 4420 (2006)
32 L.V. Zhigilei, P.B.S. Kodali, B.J. Garrison, J. Phys. Chem. B **102**, 2845 (1998)
33 A.A. Oraevsky, S.L. Jacques, J. Appl. Phys. **78**, 1281 (1995)
34 L.V. Zhigilei, Appl. Phys. A **76**, 339 (2003)
35 J.F. Mlulder, W.F. Stickle, P.E. Sobol, K.D. Bomben, *Handbook of X-ray Photoelectron Spectroscopy* (Perkin-Elmer, Eden Prairie, MN, 1992)
36 N. Alarcón, X. García, M.A. Centeno, P. Ruiz, A. Gordon, Appl. Catal. A **267**, 251 (2004)
37 J.E. Germain, in: M. Che, G.C. Bond (Eds.) *Adorption and Catalysis on Oxide Surfaces* (Elsevier, Amsterdam, 1985)
38 L. Ottaviano, F. Bussolotti, L. Lozzi, M. Passacantando, S.L. Rosa, S. Santucci, Thin Solid Films **436**, 9 (2003)
39 R.L. Frost, L. Duong, M. Weier, Spectrochim. Acta A **60**, 1853 (2004)
40 G. Busca, J. Raman Spectrosc. **33**, 348 (2002)
41 S.P.S. Porto, J.F. Scott, Phys. Rev. B **157**, 716 (1967)
42 D. Christofilos, G.A. Kouroulis, S. Ves, J. Phys. Chem. Solids **56**, 1125 (1995)
43 L.X. Brixner, H.Y. Chen, C.M. Foris, J. Solid State Chem. **45**, 80 (1982)
44 J. Tauc, A. Menth, J. Non-Cryst. Solids **8**, 569 (1972)
45 N. Saito, A. Kudo, T. Sakada, Bull. Chem. Soc. Japan. **69**, 1241 (1996)
46 M.A.M.A. Maurera, A.G. Souza, L.E.B. Soledade, F.M. Pontes, E. Longo, E.R. Leite, J.A. Varela, Mater. Lett. **58**, 727 (2004)
47 R. Grasser, A. Scharmann, Phys. Stat. Solidi A **130**, K99 (1992)
48 E. Orhan, M. Anicete-Santos, M.A.M.A. Maurera, F.M. Pontes, A.G. Souza, J. Andrès, A. Beltràn, J.A. Varela, P.S. Pizani, C.A. Taft, E. Longo, J. Solid State Chem. **178**, 1284 (2005)